Supplemetary Information

Atmospheric loss of nitrous oxide (N_2O) is not influenced by its potential reactions with OH and NO_3 radicals

A.R. Ravishankara, Anne-Laure Pele, Li Zhou, Yangang Ren, Antonia Zogka, Véronique Daële, Mahmoud Idir, Steven S. Brown, Manolis N. Romanias, and Abdelwahid Mellouki.

1. Analysis of N_2O for impurities

Nitrous oxide of two different stated purities, 99% and 99.998%, was from Air Liquide. The purity of 99% N_2O was checked for hydrocarbon impurities (alkanes and alkenes) using proton transfer reaction time-of-flight mass spectrometer (Ionicon 8000) and a Fourier transform infrared spectrometer (FTIR, Nicolet 5700). The FTIR was also used to check for CO and CO_2. An Aerodyne CAPS NO_2 monitor and CRDS was used to check for NO_2 impurities. There were no detectable impurities in the N_2O sample. The NO impurity was also measured using a CAPS NO detector to be less than 0.4 ppbv. The quoted (from Air Liquide) impurities in 99.998% pure N_2O used in this work were: H_2O < 3 ppm, O_2 < 2 ppm, C_nH_m < 1 ppm, CO < 1 ppm, CO_2 < 2 ppm, H_2 < 0.1 ppm, N_2 < 10 ppm and NO_2 < 1 ppm.

2. Apparatus used to measure the rate coefficient for the reactions of N_2O with OH and NO_3.

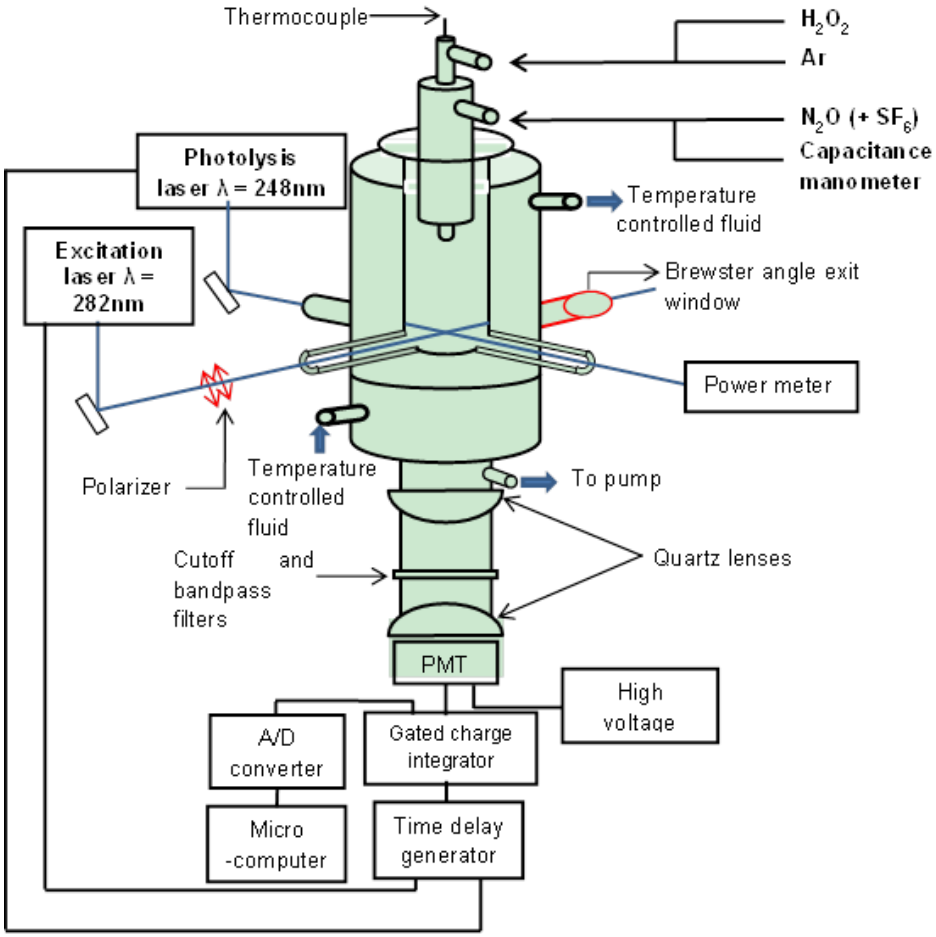

Fig. S1. Schematic diagram of the pulse laser photolysis-laser induced fluorescence (PLP-LIF) apparatus used to measure k_1.

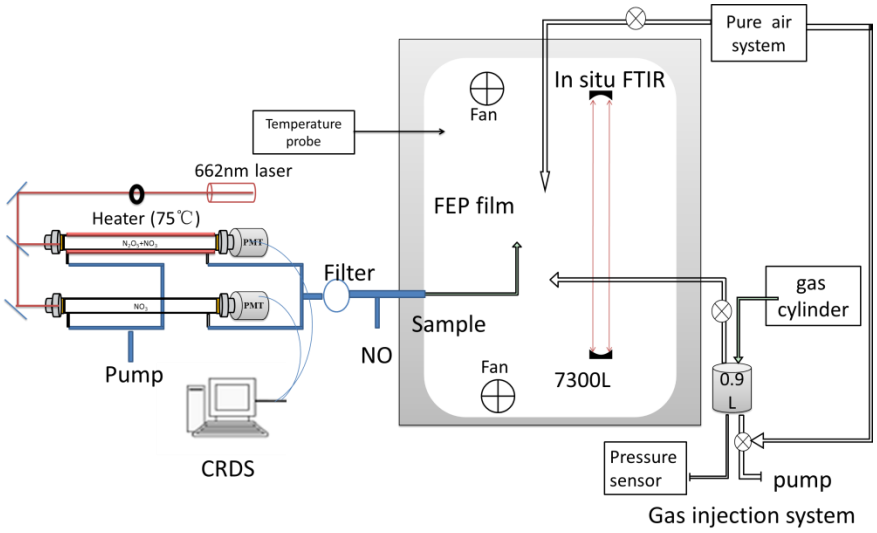

Fig. S2. Schematic diagram of the 7.3 m^3 chamber used to study the reaction of NO_3 radicals with N_2O along with the CRDS used to detect NO_3 and N_2O_5.

3. Sample N_2O calibration plot

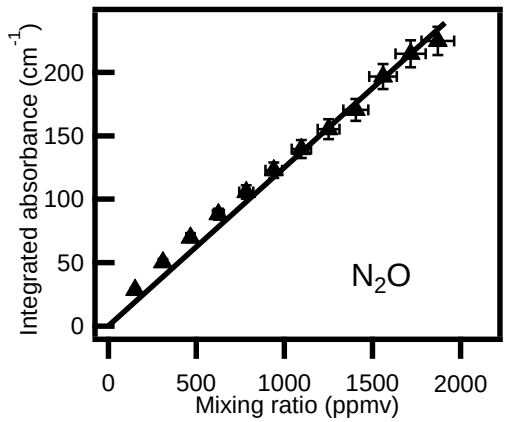

Fig. S3. Calibration curve for N_2O-A plot of the integrated absorbance of N_2O centered at 2515 cm-1 (measured as the area under the absorbance between 2620 cm^{-1} - 2410 cm^{-1}) as a function of the mixing ratio of N_2O in the chamber as determined by manometric measurements. The data was fit to a line passing through zero using a linear least-squares analysis. The uncertainties in each point, derived from multiple measurements, are shown as vertical error bars.

4. **Sample of OH temporal profiles**

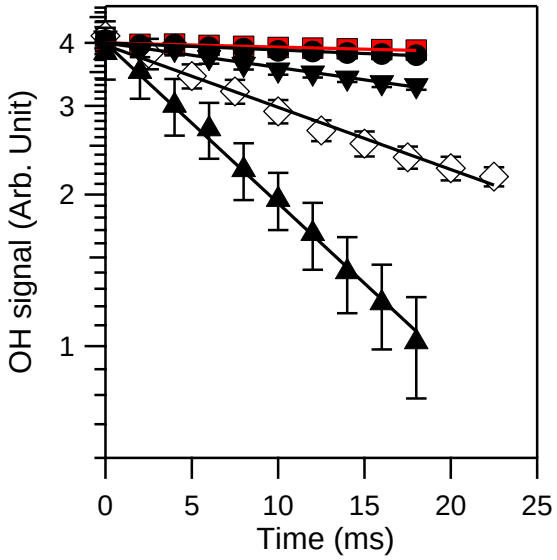

Fig. S4. Representative OH radical temporal profiles in the presence of varying concentrations of N_2O. Experimental conditions: 500 Torr (Ar) at 253 K, $\boldsymbol{[OH]_0 = 0.8 \times 10^{11}}$ molecule cm^{-3}, photolysis laser fluence = 17 mJ cm^{-2}; and N_2O concentrations (in units of 10^{17} molecule.cm^{-3}) of 0 (▲), 0.63 (◇), 2.11 (▼), 5.57 (●) and 10.8 (■). The error bars are the two standard deviations around the mean values of the measured OH signals. The lines are the weighted least-squares fits of the data where the slope yields k'. Notice that the decay rates decrease with increasing N_2O.

5. **Calculated reaction pathways and energetics**

Calculated reaction pathways and barrier

Theoretical calculations were performed to investigate the reactions of N_2O with OH and NO_3 radicals. All electronic structure calculations were carried out using the Gaussian 09 program suite [1]. The calculations were done using the quantum composite G3B3 method, [2], which is a variation of G3 theory [3]. This compound method consists of geometry optimization and vibrational frequency calculations at the B3LYP16/6-31G(d) level of theory [4]. Thereafter, a series of single-point energy calculations at four different higher levels of theory QCISD(T)/6-31G(d), MP4/6-31+G(d), MP4/6-31G(2df,p), and MP2/G3Large were performed to optimize structures. For the exothermic reaction pathways, additional calculations were carried out using the G3//MP2/aug-cc-pVDZ method. All geometry optimization and vibrational frequency calculations were done at the MP2[5]/aug-cc-pVDZ [6] level of theory. Subsequently, single-point energy calculations were calculated for the optimized structures, applying manually the G3 theory and scaling the harmonic frequencies by a factor of 0.959 as adopted from CCCBDB database. Further improvement of electronic energies were achieved by applying spin–orbit coupling corrections. In addition, the potential energy surfaces were computed by performing intrinsic reaction coordinate (IRC) calculations to verify that the located transition state (TS) structures are connected to the proper reactants and products. Each IRC calculation involved at least 50 steps at each reaction path direction (forward and reverse) with step intervals in the range of 0.04 and 0.06 au.

N_2O reaction with OH radical

*Endothermic pathway***:** The endothermic pathway to produce HNO + NO was found to proceed via the attachment of the OH radical to the nitrogen end of N_2O. Detailed description of the reaction coordinate, and the various conformations locked have been reported elsewhere [7, 8]. Here we consider the two pathways with the lowest energy barriers - also determined in the recent work of Nguyen et al - for the initial transition state conformations (Table T1 and Fig. S5) using the G3B3 composite method. In particular, OH can attack the N1-N2 double bond to form a cis-trans (TS-2) or a trans-trans (TS-3) transition state. The calculated energy barriers for the corresponding TS-2 and TS-3 are 20.6 kcal mol^{-1} and 26.7 kcal mol^{-1}. IRC calculations confirmed that both TS-2 and TS-3 are connected with the reactants as well as with post-adducts Post-2 and Post-3 unstable molecules, respectively. Thereafter another transition state is formed where H atom rotation occurs with estimated energies of 21.0 kcal mol^{-1} and 19.4 kcal mol^{-1} for TS-21 and TS-31, respectively. For these conformations, the N1-O-H fragment is situated in the plane almost perpendicular to the O-N2-N1 plane with N2-N2-O2-H and O1-N2-N1-O2 dihedral angles of 71.9^o and 179.6^o for TS-21 and 77.1^o and -2.9^o for TS-31 respectively. The HONNO post adduct is optimized for each pathway where N1 and N2 are attached via a double bond. The Post-21 unstable molecule has a cis-cis structure with an of energy 18.7 kcal mol^{-1}, while the Post-31 is a trans-cis conformation has essentially the same energy (18.8 kcal mol^{-1}). Therefore, Post-21 can easily isomerize to Post-31 thereby coupling pathways 2 and 3. Subsequently, a 1-3 hydrogen shift transition state is formed, TS-23, which appears to

have the highest barrier along the reaction coordinate (i.e., 43.2 kcal mol^{-1}). For this optimized structure, N1 and N2 are attached with a single bond (1.39 Å) while the distance of the N1-O_2 bond has been shorten. TS-23 is connected with the Post-23 HN(O)NO conformation with estimated energy of 17.3 kcal mol^{-1}. Finally, the reaction proceeds through another transition state (TS-230) where the distance of N1 and N2 atoms has been significantly elongated (i.e. 2.18 Å) and the final products can be formed. The calculated endothermic nature of the reaction was 19.2 kcal mol^{-1}, which is identical with the JPL recommended value [9]. These calculated energies and structures very consistent with those provided by Nguyen et al. [10] This is clearly a very complex sequence of reaction to produce the endothermic HNO + NO product. Also, the exothermic reaction of HNOO with NO would require going through this complex process to give OH + N_2O. Thus, we expect this reaction of HNO with NO not to give N_2O + OH.

*Exothermic pathway***:** For the exothermic pathway, the calculated reaction barrier, TS-1, is 41.5 kcal mol^{-1} and 45.3 kcal mol^{-1} at the G3B3 and G3//MP2/aug-cc-pVDZ levels, respectively. The G3B3 value of TS-1 is in good agreement with that calculated in the recent study of Nguyen et al. As seen in Table T1, the calculated exothermicity of the reaction is 24.2 and 25 kcal mol^{-1} at the G3B3 and G3//MP2/aug-cc-pVDZ levels respectively, and thus in excellent agreement with the recommended[9] value, $\Delta_f H$ (0K) = - 25.6 kcal mol^{-1}.

N_2O reaction with NO_3 radical

Endothermic pathway: The reaction coordinate of the endothermic pathway proceeds through a sequence of transition states and intermediate adducts with high energy barriers for reaction. In particular, the NO_3 radical attack the nitrogen end of N_2O. The energy barrier of the transition state (TS-2) is estimated at 35.1 kcal mol^{-1} using the G3B3 method. In addition, IRC calculations confirmed that TS-2 is directly connected with the reactants and no pre-reaction adduct is formed. A post adduct is formed where N1 and O_2 further approach while the N1-N2 and N3-O_2 bonds are even more elongated. The calculated energy of Post-2 adduct is around 1 kcal mol^{-1} lower than that for TS2 (i.e., 34.1 kcal mol^{-1}). The reaction proceeds through a second transition state (TS-21) where the N1-O_2 bond has been formed while N1 and N2 are now connected with a single bond (1.4 Å). The energy barrier of TS-21 is estimated to be 43.4 kcal mol^{-1}. Prior to product formation another post adduct conformation is formed with an energy of 40 kcal mol^{-1} where one can clearly note the presence of final products (i.e. NO_2 and NO). The estimated endothermicity of the reaction is 12.9 kcal mol^{-1} and thus close to the JPL recommended value of 12.6 kcal mol^{-1} [9].

*Exothermic pathway***:** The NO_3 radical attacks the oxygen end of N_2O. Initially a pre-reaction adduct is formed (Pre-1) with estimated energy of -2.3 kcal mol^{-1} and -1.6 kcal mol^{-1} at the G3B3 and G3//MP2/aug-cc-pVDZ levels, respectively. The energy of the transition state TS-1 was calculated to be 51.6 kcal mol^{-1} for the G3B3 composite method, and 65.4 kcal mol^{-1} with the G3//MP2/aug-cc-pVDZ theory. According to G3B3 theory TS-1 is connected with a post adduct, Post-1, with estimated energy of -

31.6 kcal mol^{-1} and then an extra energy of 1.7 kcal mol^{-1} is required to form the final products. The post adduct was not observed using the G3//MP2/aug-cc-pVDZ method.

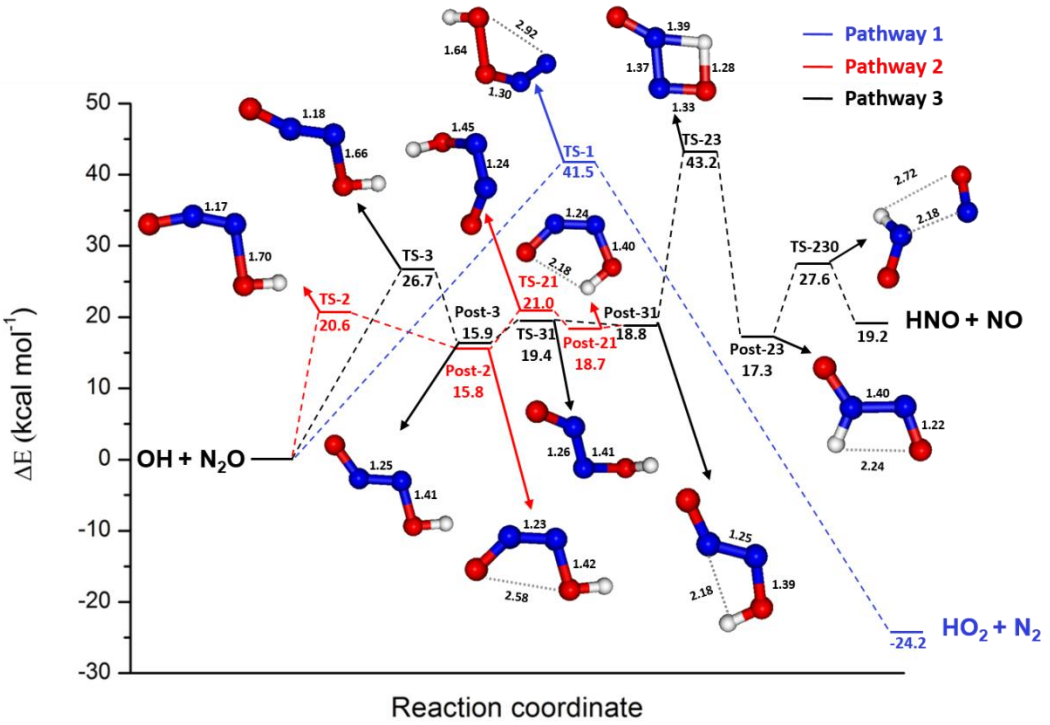

Fig. S5. Profile of the potential energy surface for the reaction of OH radical with N_2O. Structure optimizations and single point energy calculations (in kcal mol^{-1}) were carried out using the quantum composite G3B3 method. The black and red lines correspond to the endothermic pathways while the blue lines to the exothermic. The energy values noted in each conformation are in kcal mol^{-1}. The bond lengths are in Å.

Table T1. Zero point energies (kcal mol^{-1}) of various species involved in the reaction of OH radical with N_2O for the exothermic and endothermic channels. The conformation locked for the endothermic pathway 3 and the corresponding energies are given in parenthesis. For comparison purposes the zero point energies calculated using high level quantum chemistry in the recent work of Nguyen et al. are also presented.

Conformation	$OH + N_2O \rightarrow HO_2 + N_2$		
	ZPE (kcal mol^{-1})		
	G3B3	G3//MP2/aug-cc-pVDZ	mHEAT-345(Q) (Nguyen et al.)
TS-1	41.5	45.3	38.3
Products	-24.2	-25.0	-25.8
Conformation	$OH + N_2O \rightarrow HNO + NO$		
	ZPE (kcal mol^{-1})		
	G3B3		mHEAT-345(Q) (Nguyen et al.)
	Pathway 2 cis-trans	Pathway 3 trans-trans	Pathway 2 cis-trans
TS-2 (TS-3)	20.6	(26.7)	19.6
Post-2 (Post-3)	15.8	(15.9)	13.2
TS-21 (TS-31)	21.0	(19.4)	
Post-21 (Post-31)	18.7	(18.8)	
TS-23	43.2		40.2
Post-23	17.3		15.3
TS-230	27.6		27.4
Products	19.2		18.1

Reaction of N_2O with NO_3

The calculations for the energetics and reaction pathways are similar to that for OH reaction with NO_3. Instead of repeating those, we simply present the calculated potential energy surface and the associated information in Fig. S6 and Table T2.

Table T2. Zero point energies (kcal mol^{-1}) of various species involved in the reaction of NO_3 radical with N_2O for the exothermic and endothermic channels. For comparison purposes the zero point energies calculated using high level quantum chemistry in the recent work of Nguyen et al. are also presented.[11]

NO_3 + **N_2O** → N**O_2** + N_2 + **O_2**				**NO_3** + **N_2O** → N**O_2** + 2NO		
Conformation	ZPE (kcal mol^{-1})			Conformation	ZPE (kcal mol^{-1})	
	G3B3	G3//MP2/aug-cc-pVDZ	mHEAT-345(Q) (Nguyen et al.)		G3B3	mHEAT-345(Q) (Nguyen et al.)
Pre-1	-2.3	-1.6	-	TS-2	35.1	34.4
TS-1	51.6	65.4	49.9	Post-2	34.1	31.8
Post-1	-31.6	-	-	TS21	43.4	42.5
products	-29.9	-33.9	-30.6	products	12.9	12.7

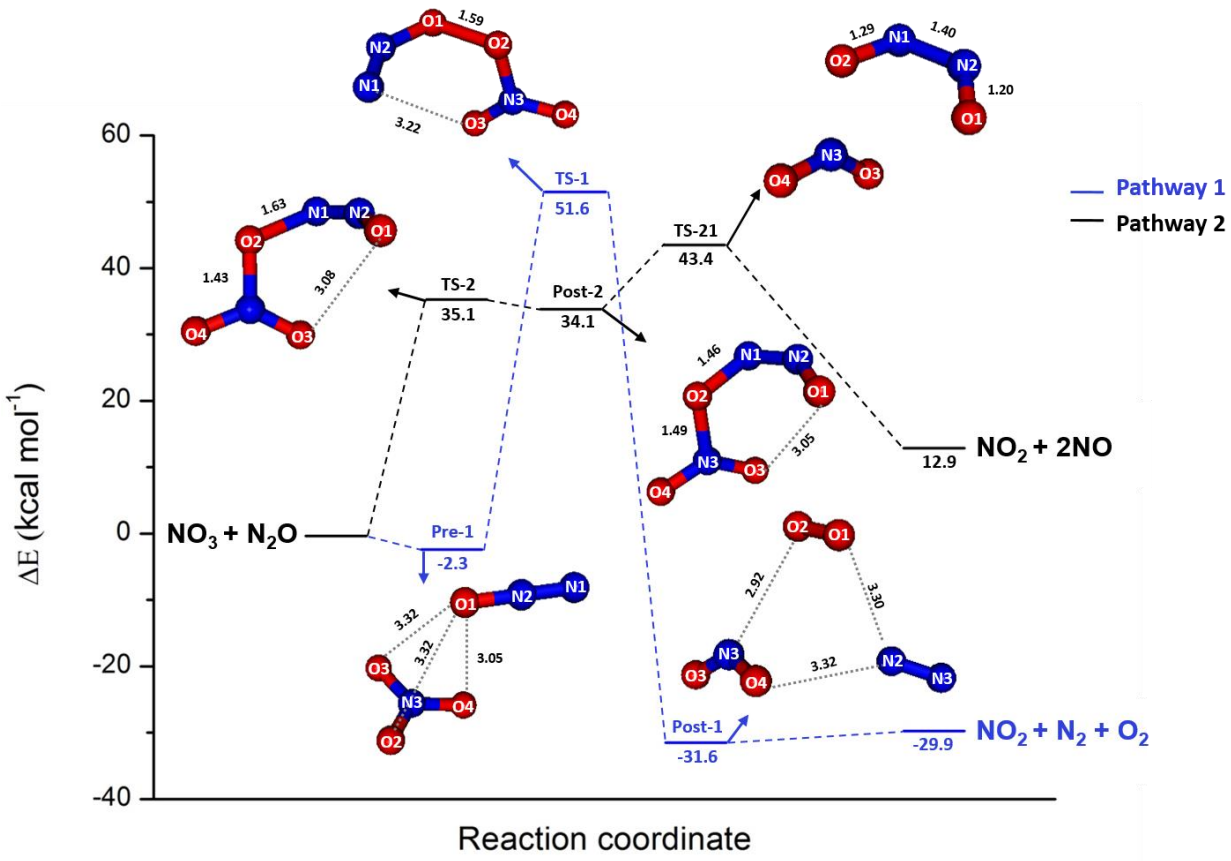

Fig. S6. Profile of the potential energy surface for the reaction of NO_3 radical with N_2O. Structure optimizations and single point energy calculations (in kcal mol^{-1}) were carried out using the quantum composite G3B3 method. The black and blue lines correspond to the endothermic and exothermic pathways respectively. The energy values noted in each conformation are in kcal mol^{-1}. The bond lengths are given in Å

References

1. M. J. Frisch, G. W. Trucks, H. B. Schlegel, G. E. Scuseria, M. A. Robb, J. R. Cheeseman, G. Scalmani, V. Barone, B. Mennucci, G. A. Petersson, H. Nakatsuji, M. Caricato, X. Li, H. P. Hratchian, A. F. Izmaylov, J. Bloino, G. Zheng, J. L. Sonnenberg, M. Hada, M. Ehara, K. Toyota, R. Fukuda, J. Hasegawa, M. Ishida, T. Nakajima, Y. Honda, O. Kitao, H. Nakai, T. Vreven, J. A. Montgomery, J. E. Peralta, F. Ogliaro, M. Bearpark, J. J. Heyd, E. Brothers, K. N. Kudin, V. N. Staroverov, R. Kobayashi, J. Normand, K. Raghavachari, A. Rendell, J. C. Burant, S. S. Iyengar, J. Tomasi, M. Cossi, N. Rega, J. M. Millam, M. Klene, J. E. Knox, J. B. Cross, V. Bakken, C. Adamo, J. Jaramillo, R. Gomperts, R. E. Stratmann, O. Yazyev, A. J. Austin, R. Cammi, C. Pomelli, J. W. Ochterski, R. L. Martin, K. Morokuma, V. G. Zakrzewski, G. A. Voth, P. Salvador, J. J. Dannenberg, S. Dapprich, A. D. Daniels, Farkas, J. B. Foresman, J. V. Ortiz, J. Cioslowski and D. J. Fox, Wallingford CT2009.
2. A. G. Baboul, L. A. Curtiss, P. C. Redfern and K. Raghavachari, *The Journal of Chemical Physics*, 1999, **110**, 7650-7657.
3. L. A. Curtiss, K. Raghavachari, P. C. Redfern, V. Rassolov and J. A. Pople, *The Journal of Chemical Physics*, 1998, **109**, 7764-7776.
4. M. M. Francl, W. J. Pietro, W. J. Hehre, J. S. Binkley, M. S. Gordon, D. J. DeFrees and J. A. Pople, *The Journal of Chemical Physics*, 1982, **77**, 3654-3665.
5. C. Møller and M. S. Plesset, *Physical Review*, 1934, **46**, 618-622.
6. R. A. Kendall, T. H. D. Jr. and R. J. Harrison, *The Journal of Chemical Physics*,

1992, **96**, 6796-6806.

7. S. W. Bunte, B. M. Rice and C. F. Chabalowski, *The Journal of Physical Chemistry A*, 1997, **101**, 9430-9438.

8. A. M. Mebel, K. Morokuma, M. C. Lin and C. F. Melius, *Journal of Physical Chemistry*, 1995, **99**, 1900-1908.

9. J. B. Burkholder, S. P. Sander, J. Abbatt, J. R. Barker, R. E. Huie, C. E. Kolb, M. J. Kurylo, V. L. Orkin, D. M. Wilmouth and P. H. Wine, ed. J. P. L. JPL Publication 15-10, Pasadena,2015.

10. T. L. Nguyen, A. R. Ravishankara and J. F. Stanton, *Chemical Physics Letters*, 2018, **708**, 100-105.

11. T. L. Nguyen, M. N. Romanias, A. R. Ravishankara, A. M. Zaras, P. Dagaut and J. F. Stanton, *Chemical Physics Letters*, 2019, **731**, 136605.